ISSN 1070-3284, Russian Journal of Coordination Chemistry, 2006, Vol. 32, No. 7, pp. 504–510. © Pleiades Publishing, Inc., 2006.

Crystal Structure and Thermodecomposition Kinetics of a Three-Dimensional Supramolecular Mn Complex with 8-Hydroxyquinoline[1]

L. R. Yang, C. F. Bi, Y. H. Fan, S. Q. Liu, F. Guo, and X. K. Ai

College of Chemistry and Chemical Engineering, Ocean University of China, Qingdao, China

Received July 4, 2005

Abstract—A three-dimensional supramolecular complex, $[Mn(8\text{-}OHQ)_3] \cdot CH_3OH$ (8-OHQ is 8-hydroxyquinoline), $C_{28}H_{22}MnN_3O_4$, was synthesized in methanol, and its crystal structure was determined by X-ray crystallography. The crystals are triclinic, space group $P\bar{1}$, a = 10.823(2) Å, b = 13.222(3) Å, c = 17.283(3) Å, α = 90.03(3)°, β = 93.15(3)°, γ = 92.58(3)°, V = 2467.0(8) Å^3, Z = 4, $F(000)$ = 1072, ρ = 1.399 g/cm^3, μ = 0.575 mm^{-1}. Hydrogen bonds and intermolecular interactions, which are observed in the complex, stabilize its structure. The thermal decomposition kinetics of the complex was investigated under nonisothermal conditions using the Achar differential method and the Coats–Redfern integral method.

DOI: 10.1134/S1070328406070074

INTRODUCTION

Manganese is essential in the metabolic processes of organisms as a micronutrient. Reports have shown that Mn affects several fundamental processes in the mobilization and activation of immunoactive haemocytes. Manganese plays an important role in antioxidant defences, being a necessary component of mitochondria enzymes, such as superoxide dismutase (MnSOD), and activates a large number of other enzymes. It also affects the central nervous system and causes the disorder manganism [1–3]. Manganese peroxidase is considered to catalyze the H_2O_2-dependent oxidative degradation of lignin. Experiments have proved that the Mn^{2+}/Mn^{3+} couple serves as a redox mediator in the oxidation phenolic lignin substructures [4]. As an excellent and useful ligand, 8-hydroxyquinoline (**8-OHQ**) presents many bioactivities and pharmacological activities, such as antibacterial, antitumor, antiphlogistic, and adjusting the metabolism of organism, etc. [5–7]. It is widely used in the separation and analysis of metal ions as well [8].

The quantitative structure activity relationship (**QSAR**) shows that planar molecules can selectively be intercalated in certain sites in nucleic acid, whose complexes can be used as the structural probes of nucleic acid to expose the mechanism of metal–enzyme acting on nucleic acid [9]. 8-OHQ gives a nearly planar structure with conjugation, and its complexes can have potential applications as mentioned above. The $[Mn(8\text{-}OHQ)_3] \cdot CH_3OH$ complex was synthesized through a special method, for which the characteristic results of IR spectra, elemental analysis, and crystal structure are reported.

EXPERIMENTAL

Reagents. Taurine was BR (Biochemical Reagent). Manganese acetate, potassium hydroxide, 8-hydroxyquinoline, methanol, and other solvents were AR (Analysis Reagent) grade and were used without further purification.

Preparation of the Schiff base ligand. Taurine (0.01 mol) and potassium hydroxide were added to methanol (15 ml) to make a pellucid solution. At 50°C, it was slowly dripped into the methanol solution (15 ml) containing 2-thenyl formaldehyde (0.01 mol). The mixture was stirred for 0.5 h to give a silvery white and flake-shape precipitate. The product was collected by filtration, washed several times with anhydrous ethanol, and dried under vacuum. Thus, the taurine-2-thenyl formaldehyde Schiff base (**TTFS**, $C_7H_8NS_2O_3K \cdot H_2O$) ligand was produced. The yield of TTFS was 88.6%.

Anal. calcd (%): C, 30.50; H, 3.62; N, 5.11; S, 19.00
For $C_7H_8NS_2O_3K \cdot H_2O$
found (%): C, 30.44; H, 3.58; N, 5.18; S, 19.53.

IR data (KBr pellets; ν, cm^{-1}): 3438 (O–H), 1640 (C=N), 1044.3, 1165.2, 1186.7 (SO_3).

Preparation of the complex. TTFS (0.5 mmol) in MeOH (15 ml) was dripped into the solution of $Mn(CH_3COO)_2 \cdot 4H_2O$ (the same molar ratio with the anterior) in MeOH (15 ml). The reaction mixture was stirred at 50°C. Two hours later, 8-OHQ (0.5 mmol in

[1] The text was submitted by the authors in English.

10 ml of anhydrous ethanol) was dripped into the mixture, continuously to be stirred at the same temperature for 8 h. The brown solution obtained was filtered, and the filtrate was left to stand for slow evaporation at room temperature. After 7 days, deep brown crystals were formed. Single crystals suitable for X-ray analysis were obtained by recrystallization from anhydrous ethanol.

Anal. calcd (%): C, 64.69; H, 4.24; N, 8.09.
For $[Mn(8\text{-}OHQ)_3] \cdot CH_3OH$
found (%): C, 64.27; H, 4.19; N, 8.13.

Physical measurements. Elemental analyses were performed on a Perkin–Elmer 240C elemental analyzer. IR spectra were recorded in the 4000–400 cm^{-1} region using KBr pellets on an AVATAR 360 FT-IR spectrometer, and the crystal structure was determined on a SMART CCD diffractometer. Thermogravimeteric measurements were made using a Perkin–Elmer TGA7 thermogravimeter. The heating rate was programmed to be 10 K/min with the protecting stream of N_2 flowing at 40 ml/min.

X-Ray crystallographic determination. The selected crystal of dimensions $0.40 \times 0.32 \times 0.24$ mm was mounted on a Bruker Smart CCD X-ray single-crystal diffractometer. Reflection data were at 293(2) K using graphite monochromated MoK_α-radiation (λ = 0.71073 Å), $\omega/2\theta$ scan mode. All 4747 independent reflections were collected in a range of $1.18° \le \theta \le 27.16°$, of which 3216 reflections with $I = 2\sigma(I)$ were considered to be observed and used in the subsequent refinement. The correction for Lp factors and empirical absorption were applied to the data. The structure were solved by direct methods and Fourier syntheses. Positional and thermal parameters were refined by the full-matrix least-squares method on F^2 using the SHELXTL software package [10]. The final least-square cycle of refinement gave $R = 0.0489$, $wR = 0.1598$, the weighting scheme $w = 1/[\sigma^2(F_o^2) + (0.0910P)^2 + 1.4692P]$, where $P = (F_o^2 + 2F_c^2)/3$. A summary of the key crystallographic information is given in Table 1.

Table 1. Summary of crystallographic data for the complex $[Mn(8\text{-}OHQ)_3] \cdot CH_3OH$

Empirical formula	$C_{28}H_{22}MnN_3O_4$
Formula weight	2077.70
Crystal system	Triclinic
Space group	$P\bar{1}$
a, Å	10.823(2)
b, Å	13.222(3)
c, Å	17.283(3)
α, deg	90.03(3)
β, deg	92.58(3)
Z	4
Volume, Å^3	2467.0(8)
$F(000)$	1020
Limiting indices	$0 \le h \le 12$, $-15 \le k \le 0$, $-20 \le l \le 20$
Reflections collected/unique	4747/4747; (R_{int} = 0.0054)
Refinement method	Full-matrix least-squares on F^2
Data/restraints/parameters	4747/21/681
Goodness-of-fit on F^2	1.216
R indices (all data)	$R_1 = 0.0852$, $wR_2 = 0.1787$
Largest diff. peak and hole, eÅ^{-3}	0.428 and –0.359

RESULTS AND DISCUSSION

Description of crystal structure. Our anticipative product was the complex of Mn(III) with taurine-2-thenyl formaldehyde Schiff base (TTFS)-Mn(III)-8-OHQ. Accidentally, the $[Mn(8\text{-}OHQ)_3] \cdot CH_3OH$ complex and its crystal were obtained, owing to the following facts: *a*) the weaker coordination ability of $-SO_3H$ in TTFS; *b*) the steric effect of 8-OHQ and its stronger coordination ability (compared to the former). TTFS might be substituted by 8-OHQ to form the complex, and TTFS acts as a dropping-out group. Here, TTFS presented a chemically modification action in the reaction. To validate our conclusion, a reaction between 8-OHQ and manganese acetate was performed under the same conditions. As a result, the complex was not obtained.

Non-hydrogen fractional atomic coordination and equivalent isotropic temperature factors, selected bond lengths, band angles, and intermolecular interaction distances of the complex are listed in Tables 2 and 3, respectively. The crystal structure and molecular packing drawing of the complex are shown in Figs. 1 and 2.

Structural units in the crystal are two crystallographically independent monomeric complex molecules $[Mn(8\text{-}OHQ)_3]$ and solvate methanol molecules. The structures and geometric parameters of two complexes with the Mn(1) and Mn(2) atoms are similar. Further descriptions are for molecule with the Mn(1) atom.

Figure 1 shows that the central Mn(III) atom is bound by the O and N atoms belonging to 8-OHQ (O(1), N(1), O(2), N(2), O(3), N(3)) to form a six-coordinate complex with three five-membered chelate rings (ring 1: Mn(1)–O(1)–C(6)–C(5)–N(1); ring 2: Mn(1)–O(2)–C(15)–C(14)–N(2); ring 3: Mn(1)–O(3)–C(24)–C(23)–N(3)). The Mn atoms in the five-membered chelate rings deviate from the plane for a mean value of 0.0051 Å. The central Mn(III) atom adopts a distorted octahedron geometry with O(1), O(2), O(3), N(3), lying on the equatorial plane. The corresponding bond angles are O(1)Mn(1)O(2) 94.73(3)°, O(1)Mn(1)N(3)

Table 2. Non-hydrogen fractional atomic coordination ($\times 10^4$) and equivalent isotropic temperature factors ($\times 10^3$) ($U_{eq} = (1/3)\Sigma_i\Sigma_j U_{ij} a_i^* a_j^* a_i a_j$) for complex $[Mn(8\text{-}OHQ)_3] \cdot CH_3OH$

Atom	*x*	*y*	*z*	U_{eq}, Å^2	Atom	*x*	*y*	*z*	U_{eq}, Å^2
Mn(1)	4268(1)	9812(1)	–7423(1)	36(1)	C(7)	1146(10)	9680(8)	–8537(5)	69(5)
Mn(2)	10731(1)	14814(1)	–7576(1)	37(1)	C(8)	953(13)	9370(9)	–9292(6)	92(6)
O(1)	2579(5)	9936(5)	–7629(2)	47(2)	C(9)	1865(14)	8996(10)	–9829(6)	104(7)
O(2)	4098(6)	8486(4)	–6991(2)	48(2)	C(10)	3588(9)	11020(7)	–5736(4)	53(4)
O(3)	6017(7)	9841(5)	–7370(3)	51(3)	C(11)	3353(10)	11049(7)	–4917(4)	60(4)
O(4)	12429(5)	14929(4)	–7371(2)	51(2)	C(12)	3237(10)	10150(8)	–4517(4)	60(4)
O(5)	10906(5)	13481(4)	–8010(2)	46(2)	C(13)	3392(9)	9229(7)	–4928(4)	50(4)
O(6)	8984(6)	14844(4)	–7632(3)	44(2)	C(14)	3642(8)	9281(6)	–5753(3)	38(3)
O(7)	4539(9)	15499(7)	–8352(6)	122(5)	C(15)	3845(8)	8399(6)	–6220(4)	45(3)
O(8)	–404(9)	9482(7)	–3333(5)	119(5)	C(16)	3787(9)	7476(7)	–5848(4)	50(3)
N(1)	4467(7)	9252(5)	–8653(3)	45(3)	C(17)	3524(9)	7435(7)	–5017(4)	62(4)
N(2)	3737(7)	10193(5)	–6134(3)	39(3)	C(18)	3322(10)	8270(8)	–4567(4)	59(4)
N(3)	4575(7)	11290(6)	–7736(3)	38(3)	C(19)	3792(10)	11999(7)	–7921(4)	52(4)
N(4)	10545(7)	14253(6)	–6341(3)	45(3)	C(20)	4229(13)	12992(10)	–8118(4)	65(5)
N(5)	11273(7)	15185(5)	–8859(3)	41(3)	C(21)	5425(10)	13230(9)	–8132(4)	60(4)
N(6)	10420(7)	16299(6)	–7263(3)	34(3)	C(22)	6302(12)	12507(9)	–7913(4)	46(5)
C(1)	5399(10)	8911(7)	–9136(4)	65(4)	C(23)	5805(11)	11544(8)	–7741(3)	36(4)
C(2)	5303(12)	8583(9)	–9886(5)	72(5)	C(24)	6549(11)	10718(8)	–7536(3)	42(4)
C(3)	4168(14)	8604(9)	–10133(5)	85(6)	C(25)	7815(12)	10929(9)	–7546(4)	52(5)
C(4)	3114(12)	8965(8)	–9630(4)	69(5)	C(26)	8287(13)	11888(9)	–7710(4)	60(5)
C(5)	3318(9)	9273(7)	–8886(4)	51(4)	C(27)	7570(10)	12672(10)	–7895(4)	58(5)
C(6)	2320(9)	9635(7)	–8327(4)	49(3)	C(28)	9586(11)	13913(8)	–5870(4)	66(5)

89.7(3)°, O(2)Mn(1)O(3) 94.3(3)°, and O(3)Mn(1)N(3) 81.9(3)°. The sum of bond angles (nearly 360°) indicates that the four atoms (O(1), O(2), O(3), N(3)) are almost coplanar. The bond angles of those atoms situated on the diagonals are O(1)Mn(1)O(3) 169.6(2)°, O(2)Mn(1)N(3) 171.7(2)°, which deviate from 180°. The bonds along the axis (Mn(1)–N(1) (2.275(5) Å) and Mn(1)–N(2) (2.390(5) Å)) are distinctly longer than those of the equatorial plane (Mn(1)–O(1) 1.857(5), Mn(1)–O(2) 1.911(6), Mn(1)–O(3) 1.890(8),

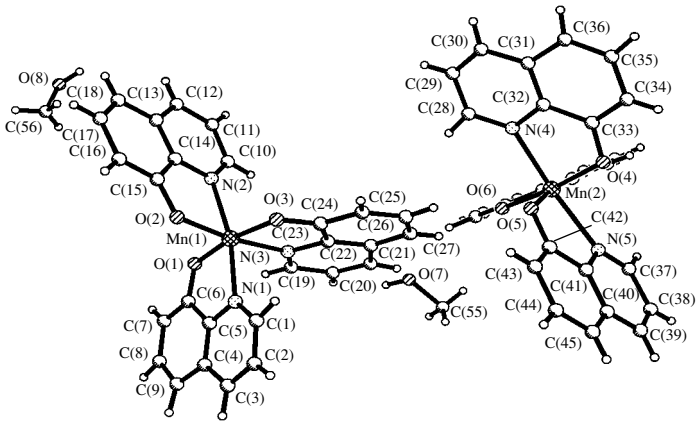

Fig. 1. Crystal structure of the complex $[Mn(8\text{-}OHQ)_3] \cdot CH_3OH$.

Table 3. Selected bond lengths (d) and angles (ω) for complex $[Mn(8\text{-}OHQ)_3] \cdot CH_3OH$

Bond	d, Å	Bond	d, Å	Bond	d, Å
Mn(1)–O(1)	1.857(5)	Mn(1)–N(1)	2.275(5)	Mn(2)–O(5)	1.935(5)
Mn(1)–O(3)	1.890(8)	Mn(1)–N(2)	2.390(5)	Mn(2)–N(6)	2.083(7)
Mn(1)–O(2)	1.911(6)	Mn(2)–O(4)	1.852(6)	Mn(2)–N(4)	2.277(6)
Mn(1)–N(3)	2.046(9)	Mn(2)–O(6)	1.890(6)	Mn(2)–N(5)	2.370(6)
Angle	ω, deg	Angle	ω, deg	Angle	ω, deg
O(1)Mn(1)O(3)	169.6(2)	O(1)Mn(1)N(2)	82.3(2)	O(5)Mn(2)N(6)	171.75(19)
O(1)Mn(1)O(2)	94.7(3)	O(3)Mn(1)N(2)	104.5(2)	O(4)Mn(2)N(4)	88.3(2)
O(3)Mn(1)O(2)	94.3(3)	O(2)Mn(1)N(2)	78.7(2)	O(6)Mn(2)N(4)	86.0(2)
O(1)Mn(1)N(3)	89.7(3)	N(3)Mn(1)N(2)	95.0(2)	O(5)Mn(2)N(4)	94.8(2)
O(3)Mn(1)N(3)	81.9(3)	N(1)Mn(1)N(2)	169.6(3)	N(6)Mn(2)N(4)	92.2(2)
O(2)Mn(1)N(3)	171.7(2)	O(4)Mn(2)O(6)	169.9(2)	O(4)Mn(2)N(5)	83.0(2)
O(1)Mn(1)N(1)	90.4(2)	O(4)Mn(2)O(5)	89.5(2)	O(6)Mn(2)N(5)	103.7(2)
O(3)Mn(1)N(1)	83.8(2)	O(6)Mn(2)O(5)	99.2(3)	O(5)Mn(2)N(5)	77.5(2)
O(2)Mn(1)N(1)	94.6(2)	O(4)Mn(2)N(6)	95.0(3)	N(6)Mn(2)N(5)	96.2(2)
N(3)Mn(1)N(1)	92.3(2)	O(6)Mn(2)N(6)	77.0(3)	N(4)Mn(2)N(5)	168.41(17)

and Mn(1)–N(3) 2.046(9) Å) mainly due to the Jahn–Teller effect [11].

Figure 2 illustrates a perspective view of the crystal packing in the unit cell. The most prominent structural feature of the complex is that it assembles a three-dimensional supramolecular network through potentially weak C–H···O hydrogen bonds, intermolecular interactions, and C–H···π (C(20)–H(20*A*)···Cg(5) and C(47)–H(47*A*)···Cg(2), etc.) supramolecular interactions [12]. Furthermore, the weaker π–π stacking interaction, such as Cg(2)–Cg(12), Cg(14)–Cg(12), and Cg(17)–Cg(9), are possible [13, 14], as can be deduced from the short contact distances 3.9521, 3.9050, and 3.9970 Å, respectively (see Table 4). As a result, π–π stacking occurs omnipresently, which stabilizes the structure of the complex and is beneficial to the transmission of electric charges [15]. In the unit cell, the four Mn atoms are coplanar and occupy the parallelogram vertexes, respectively.

Spectroscopic studies. 8-OHQ owns 5 characteristic absorption peaks: ν(O–H) (3088), δ(O–H) (1210), ν(C=N) (1587), ν(C–O) (1104), and ν(C=C) (1476 cm^{-1}).

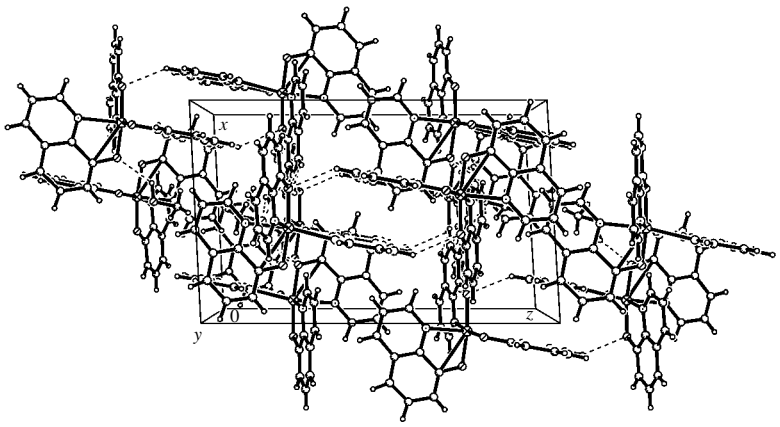

Fig. 2. Packing drawing of the complex $[Mn(8\text{-}OHQ)_3] \cdot CH_3OH$.

Table 4. Intermolecular interaction distances (Å) for complex $[Mn(8\text{-}OHQ)_3] \cdot CH_3OH$

D–H···A[1]	Symm. A	H···A, Å	D···A, Å	Angle D–H···A, deg	Cg–Cg, Å
C(12)–H(12*A*)···O(3)	$1 - x, -y, 1 - z$	2.51	3.31	145	
C(25)–H(25*A*)···O(8)	$1 + x, y, z$	2.52	3.18	128	
C(27)–H(27*A*)···O(6)	$1 + x, y, z$	2.36	3.21	152	
C(39)–H(39*A*)···O(6)	$-x, 1 - y, -z$	2.50	3.32	148	
C(48)–H(48*A*)···O(8)	$x, 1 + y, z$	2.44	3.15	133	
C(52)–H(52*A*)···O(7)	$-1 + x, y, z$	2.56	3.20	126	
C(54)–H(54*A*)···O(3)	$-1 + x, 1 + y, z$	2.47	3.33	154	
C(20)–H(20*A*)···Cg(5)[2]	x, y, z	3.01	3.87	154	
C(47)–H(47*A*)···Cg(2)	$x, 1 + y, z$	2.85	3.70	152	
C(55)–H(55*A*)···Cg(7)	$x, 1 + y, z$	3.31	3.65	106	
C(55)–H(55*C*)···Cg(7)	$x, 1 + y, z$	3.38	3.65	100	
C(56)–H(56*A*)···Cg(10)	x, y, z	3.04	3.68	130	
C(56)–H(56*C*)···Cg(8)	x, y, z	3.18	3.85	133	
Cg(2)–Cg(12)$^{\#}$[3]	$x, -1 + y, z$				3.95
Cg(14)–Cg(12)	$x, -1 + y, z$				3.91
Cg(17)–Cg(9)	x, y, z				4.00

[1]D–H 0.93 Å.

[2]Cg(2): Mn(1)–O(2)–N(2)–C(14)–C(15); Cg(5): Mn(2)–O(5)–N(5)–C(41)–C(42); Cg(7): N(1)–C(1)–C(2)–C(3)–C(4); Cg(8): N(2)–C(10)–C(11)–C(12)–C(13)–C(14); Cg(9): N(3)–C(19)–C(20)–C(21)–C(22)–C(23); Cg(10): N(4)–C(28)–C(29)–C(30)–C(31)–C(32); Cg(12): N(6)–C(46)–C(47)–C(48)–C(49)–C(50); Cg(14): C(13)–C(14)–C(15)–C(16)–C(17)–C(18); Cg(17): C(40)–C(41)–C(42)–C(43)–C(44)–C(45); C(55), C(56): MeOH; C(20), Cg(2), Cg(7), Cg(8), Cg(9), and Cg(14) belong to Mn(1); C(47), Cg(5), Cg(10), and Cg(12) belong to Mn(2).

[3]The center-to-center distance between two adjacent rings; symmetry transformations used to generate equivalent atoms: $^{\#}x, -1 + y, z$.

The bands ν(O–H) and δ(O–H) disappear after the formation of the complex, which indicates that the hydroxy O atoms are coordinated with Mn, while ν(C=N) shifts from 1587 to 1572 cm^{-1} showing that the N atoms participate in coordination. In addition, ν(C–O) shifts to 1107 cm^{-1}, which notarizes the result simultaneously [16].

Thermal decomposition kinetics studies. The *TG* and *DTG* curves of the complex are shown in Fig. 3, which indicates that the complex decomposes in two

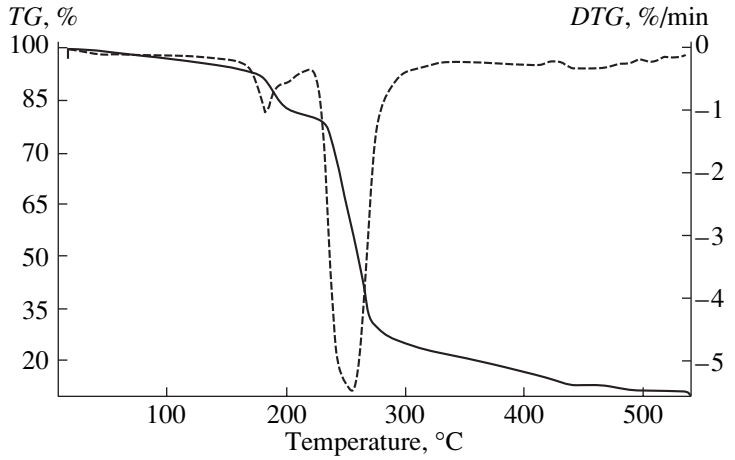

Fig. 3. *TG–DTG* curves of the complex $[Mn(8\text{-}OHQ)_3] \cdot CH_3OH$.

Table 5. Data for step (2) of the thermodecomposition of the complex $[Mn(8\text{-}OHQ)_3] \cdot CH_3OH$ obtained from the *TG* and *DTG* curves [19]

T_i, K	α_i	$(d\alpha/dt)_i$
503	0.0239	0.0552
510	0.1074	0.1419
515	0.2176	0.1828
520	0.3495	0.1991
523	0.4145	0.2034
525	0.4651	0.2058
526	0.4900	0.2068
527	0.5158	0.2077
528	0.5421	0.2085
529	0.5693	0.2074
530	0.5965	0.2062
531	0.6228	0.2031
533	0.6759	0.1898
536	0.7501	0.1653
541	0.8447	0.1009
546	0.8939	0.0469
556	0.9406	0.0158

steps. The first weight loss step has a decomposition temperature range of 165–205°C with a weight loss of 6.13%, which corresponds to the loss of four molecules of methanol (calcd 6.16%). The fact suggests that methanol is closely bound to the complex by hydrogen bonds. The second weight loss step has a decomposition temperature range of 205–500°C with a weight loss of 81.71% corresponding to the loss of twelve molecules of 8-OHQ (calcd 83.17%). The fact that 8-OHQ was lost at a higher temperature suggests that it is coordinated with the metal ion. A value of 11.62% of the original sample remained with its calculated weight percentage of 10.59%, and Mn is the final residue.

On the basis of 30 kinetic functions, in both differential and integral forms commonly used in recent reports [17, 18], the nonisothermal kinetics of the second step was investigated using the Achar differential method [19] and the Coats–Redfern integral method [20].

The original kinetic data for step (2) obtained from the *TG* and *DTG* curves are listed in Table 5, in which T_i is the temperature at any point i on the *TG* and *DTG* curves, and α_i is the corresponding decomposition rate. Equation $(d\alpha/dt)_i = [\beta/(W_0 - W_1)](dW/dT)_i$ in which $(dW/dT)_i$ is the height of the peak in the *DTG* curve, β is the heating rate, and W_0 and W_1 are the initial and final weight at the stage, respectively.

The calculated kinetic parameters (***E, A***) and correlation coefficients (***r***) of step (2) are listed in Table 6.

The results obtained from the two different methods are approximately the same when based on function no. 18 for step (2) (Table 6). The kinetic equation is expressed as follows: $d\alpha/dt = Ae^{-E/RT}(1 - \alpha)^2$, E = 265.62 kJ/mol, $\ln A = 47.43$.

Table 6. Results of the analysis of the data for Step (2) in Table 5 by the differential method by Achar (I) and the integral method by Coats–Redfern (II)

Number kinetic function	E, kJ/mol	$\ln A$	r	E, kJ/mol	$\ln A$	r
	I			II		
1	282.35	50.06	0.8691	89.54	18.24	0.4118
2	309.61	55.82	0.8920	141.62	29.84	0.6050
3	321.54	57.13	0.9018	164.82	33.78	0.6776
4	346.14	62.93	0.9194	208.20	43.99	0.7820
5	259.52	42.37	0.8545	57.01	8.21	0.2837
6	432.91	83.34	0.9621	338.37	74.61	0.9350
7	188.86	30.05	0.9399	74.18	15.87	0.6718
8	122.98	15.19	0.9372	8.25	0.60	0.1343
9	90.04	7.75	0.9343	–24.69	–7.12	0.4349
10	57.10	0.32	0.9278	–57.63	–14.96	0.8070
11	282.85	50.00	0.8691	89.54	18.24	0.4118
12	159.69	22.48	0.9024	9.05	–0.14	0.0898
13	168.68	24.20	0.9156	30.75	4.56	0.3106
14	136.78	17.76	0.8620	–56.03	–14.75	0.4236
15	64.00	1.61	0.8463	–128.81	–31.59	0.8433
16	39.74	–3.77	0.8280	–153.07	–37.38	0.9091
17	27.61	–6.46	0.8068	–165.20	–40.36	0.9318
18	266.95	48.38	0.9870	264.29	46.48	0.9716
19	56.30	0.77	0.9387	139.21	30.48	0.9076
20	88.26	6.99	0.8544	–104.55	–25.92	0.7421
21	386.50	74.63	0.9425	89.54	18.24	0.4118
22	584.15	119.22	0.9434	469.42	106.14	0.9089
23	781.79	163.81	0.9438	667.06	151.01	0.9204
24	251.54	46.70	0.9495	334.46	77.79	0.9923
25	173.44	25.03	0.9219	41.59	6.82	0.4158
26	105.10	10.91	0.7889	–186.19	–44.68	0.7591
27	85.04	6.49	0.7328	–316.35	–74.89	0.8449
28	71.31	3.44	0.6901	–446.51	–105.32	0.8798
29	73.95	4.83	0.9070	–201.60	–47.05	0.9723
30	75.45	3.97	0.8922	–71.43	–16.43	0.9164

Supplementary materials. CCDC-273721 contains the supplementary crystallographic data for this paper.*

* These data can be obtained free of charge via www.ccdc.cam.ac.uk/data_request/cif, or by e-mailing data_request@ccdc.cam.ac.uk, or by contacting The Cambridge Crystallographic Data Centre, 12, Union Road, Cambridge CB2 1EZ, UK; fax: +44-1223-336033.

REFERENCES

1. Hernroth, B., Susanne, P., *et al*., *Aquatic Toxicology,* 2004, vol. 70, p. 223.
2. Hirata Yoko, *Neurotoxicol. Teratol*., 2002, vol. 24, p. 639.
3. Iregren, A., *Neurotoxicol. Teratol.,* 1990, vol. 12, p. 673.
4. Yasuhiko Asada, Akira Watanabe, Toshikazu Irie, *et al*., *Biochim. Biophys. Acta, Ser. Protein Struct. Mol. Enzymol.,* 1995, vol. 1251, no. 2, p. 205.
5. Tripathi, S.P., Kumar, R., and Chaturvedi, G.K., *J. Indian Chem. Soc.,* 1984, vol. 61, no. 10, p. 847.
6. Jeffrey, M.B., Hansch, C., Silipo, C., *et al., Chem. Rev.,* 1984, vol. 84, p. 333.
7. Sharma, R.C., Tripathi, S.P., Sujata Khanna Km., and Sharma, R.S. *Curr. Sci*., 1981, vol. 50, no. 17, p. 748.
8. Li Chang-zheng, Wang Xue-zhi, Tang Ning, *et al*., *Chem. Res. Appl.,* 1994, vol. 6, no. 2, p. 66.
9. Zhang Li-he, *Druggery Research on Nucleic Acid as Target,* Beijing (China): Science Press, 1997, p. 156.
10. Sheldrick, G.M., *SHELXTL, version 5. Reference Manual, Siemens Analytical X-ray Systems,* Inc., I (USA), 1996.
11. Zhou Bei-chuan, Kou Hui-zhong, Gao Dong-zhao, *et al., Chin. J. Struct. Chem*., 2002, vol. 21, p. 549.
12. Glusker, J. P., Lewis, M., and Rossi, M., C*rystal Structure Analysis for Chemists and Biologists,* New York: VCH Publishers Inc., 1994.
13. Hunter, R.H., Haueisen, R.H., and Irving, A., *Ang. Chem. Int. Ed. Engl.,* 1994, vol. 33, no. 5 p. 566.
14. Jian Fang-fang, Hou Yu-xia, Xiao Hai-lian, *Chin. J. Inorg. Chem*., 2004, vol. 20, p. 555.
15. Alleyne, B.D., Hall, L.A., Kahwa, I. A., *et al*., *Inorg. Chem.,* 1999, vol. 38, no. 26, p. 6278.
16. Geary, W.J., *Coord. Chem. Rev.,* 1971, vol. 7, p. 81.
17. Yuzheng, L., *Thermal Analysis,* Beijing (China): Qinghua Univ. Press, 1987, p. 94.
18. Fan Yu-hua, Bi Cai-feng, and Li Jin-ying, *Synt. React. Inorg. Met.-Org. Chem*., 2003, vol. 33, no. 1, p. 137.
19. Achar, B.N., *Proceeding of International Clay Conference*, Book 1, Jerusalem, 1966, p. 67.
20. Coats, A.W. and Redfern, J.P., *Nature*, 1964, vol. 201, p. 68.